Coarse-Grained Molecular Dynamics Simulations of Stereoregular Poly(methyl methacrylate)/Poly(vinyl chloride) Blends

Chaofu Wu

Department of Chemistry and Materials Science, Hunan University of Humanities Science & Technology, Dixing Road 487, Louxing District, Loudi 417000, Hunan Province, People's Republic of China
Correspondence to: C. Wu (E-mail: xiaowu759@hotmail.com or xiaowu759@qq.com)

Received 1 July 2014; revised 20 September 2014; accepted 22 September 2014; published online 6 October 2014
DOI: 10.1002/polb.23608

ABSTRACT: The stereoregular poly(methyl methacrylate)/poly(-vinyl chloride) blends with a wide formulation range are extensively simulated using the coarse-grained (CG) molecular dynamics (MD) method. To improve the representability, the bonded CG potentials are re-parameterized against the atomistic simulated melt systems whereas the nonbonded CG potentials are adopted as developed in our previous work. Based on the CG potentials, the MD simulations reproduce all the local distributions of pure systems and the miscibility of mixed systems. Moreover, the global conformational properties are also closer to the target ones than those obtained using the previous CG potentials. The changes in density and volume upon mixing are computed together with the energies of mixing. They are all negative over the entire composition range and indicate stronger intermolecular interactions between distinct components than those between identical components. In particular, it is found that upon mixing the changes in density are insensible to chain tacticity but the changes in volume and the energies of mixing do, which quantitatively confirms that both inter-molecular interactions and free-volumes mainly contribute to the observed phase behaviors. Such models and methods reported herein can be used to quickly optimize formulations of polymer blends. © 2014 Wiley Periodicals, Inc. J. Polym. Sci., Part B: Polym. Phys. **2015**, *53*, 203–212

KEYWORDS: blends; miscibility; mixing; molecular dynamics; molecular modeling; phase behavior

INTRODUCTION Phase behavior of polymer blends remains to be an active research topic in view of its association to properties of materials. Experimentally, it is well established that miscibility of polymer blends depends upon many factors, such as molecular weight, formulation, temperature, etc. In particular, disagreements in the literature regarding miscibility of polymer blends were often attributed to differences in sample preparation methods, thermal history and characterization techniques,[1] where subtle intermolecular interactions played the key roles. One fascinating characteristic is that trivial changes in covalent structure of a monomer can lead to dramatic changes in the phase diagram.[2] The binary blend comprising poly(methyl methacrylate) (PMMA) and poly(vinyl chloride) (PVC) serves as one typical example, for which almost all experiments consistently pointed out that syndiotactic PMMA (sPMMA) was more miscible with PVC than was isotactic PMMA (iPMMA).[3] However, it is not yet quite clear how intermolecular interactions, which are indirectly detected in the experiments, influence the phase behaviors of polymer blends.

Alternatively, all-atomistic (AA) molecular simulations allow intermolecular interactions to be examined in detail. They have been extensively employed for understanding miscibility of binary polymer blends.[4–11] Generally, these AA simulations are often restricted to short chains and duration time because they are too time-consuming. Moreover, the ultimate phase behaviors of mixed systems critically depend upon the initial configurations.[9] To speed the relaxation procedure, coarse-grained (CG) models, in which several atoms are reduced to one CG bead, have been often employed for mesoscopic simulations (i.e., MesoDyn[12–15] and DPD[16,17]) and theoretical calculations.[3] However, these general-purpose models neglect most chemical details of specific polymers.

On this point, multiscale simulations have attracted much attention during the past decade.[18,19] The key elements of these simulations are systematic CG potentials, which are usually parameterized against the AA simulations.[20,21] A great variety of CG methods have been proposed to study various polymer systems.[22,23] For its simplicity and general applicability, the IBI method[24] is popular in deriving the CG potentials, which are able to exactly reproduce the target structural distributions. However, this method is relatively time-consuming for deriving the nonbonded CG potentials, and sometimes it is hard to yield the convergent solutions.

More critically, for polymer blends, the target AA simulations need to be performed on the mixed systems,[25] which make the CG potentials bias in yielding similar morphologies to the parameterized ones. This problem is usually referred to the lack of transferability of CG potentials,[26,27] which explains why such multiscale simulations were seldom reported for polymer blends.[25,28–30] Alternatively, the conditional reversible work (CRW) method has been proposed for deriving the nonbonded CG potentials,[31] which provide a true measure of the physical interaction free energies between two groups of atoms.[32] As pointed out, the derived CG potentials (i.e., CRW), in which multibody contributions from the surrounding environment are kept minimal, exhibit better transferability than the parameterised CG potentials (i.e., IBI).[21,33] Recently, we have combined the IBI and CRW methods to develop the systematically CG potentials for stereoregular PMMA/PVC blends.[34] This combined scheme is promising in that it is computationally inexpensive and the CG potentials reasonably represent both structural and energy properties.

As a rough approximation, in that work[34] the bonded CG potentials have been parameterized against the atomistic simulated single chains in a vacuum, which costs only a fraction of computational time. While capturing the tacticity effects on the miscibility, the so-obtained CG potentials can not exactly reproduce the structural distributions in the melt systems.[35] To improve the representability, in this work, the bonded CG potentials are re-parameterized against the atomistic simulated melt systems. The refined CG potentials are then extended to investigate miscibility of stereoregular PMMA/PVC blends using the molecular dynamics (MD) method. The two-fold purposes are pursued, to examine the transferability of the CG potentials to different formulations, and to understand the influences of composition and tacticity on miscibility of the mixed systems.

COMPUTATIONAL DETAILS

Investigated in this work are totally three pure systems (60iMA24, 60sMA15, and 50iVC24) and eighteen mixed systems. These polymer blends have the same total number of chains (i.e., 200) but different formulations, leading to molar fractions ranging from 0 to 1.0 every 0.1. For references thereafter, each pure system is given a brief name that consists of four parts, that is, the first is number of chains with a digit, the second denotes isotactic or syndiotactic with a character "i" or "s," the third represents type of monomer with two characters, and the fourth indicates number of monomers per chain. Similarly, each mixed system is denoted by a brief name containing two such sections that are separated by "/". For example, 100sMA15/100iVC24 represents a polymer blend comprised of 100 sPMMA chains of 15 monomers per chain and 100 iPVC chains of 24 monomers per chain.

To save the computational time, the same short chains as in the previous work[34] were investigated, that is, 15 monomers for both PMMAs and 24 monomers for PVC. Note that such a PMMA chain has almost the same mass as such a PVC chain. Single stereoregular chains were first built using the commercial Materials Studio-4.0 program (Developed by Accelrys). Using the packmol code,[36,37] such PMMA and/or PVC chains with the required numbers of chains were then packed into cubic boxes. The periodic boundary conditions (PBCs) were imposed on the models to represent the melt systems. The dimensions of boxes were initially defined to give a density close to 1000 kg/m^3. The bonded CG potentials were developed using the VOTCA-1.3-dev code,[38] and all the following AA and CG simulations were performed using the GROMACS-4.5.4 code.[39,40]

According to the combined scheme,[34] the CRW method[31] is first employed to derive the non-bonded CG potentials, and the IBI method[24] is then used to derive the bonded CG potentials. The nonbonded CG potentials are obtained by integrating the constraint forces from some distance to cut-off whereas the bonded CG potentials were parameterized to reproduce the bonded distributions (i.e., bond length, bond angle, dihedral angle). More details can be referred to our previous work.[34] In this work, the previously developed nonbonded CG potentials were adopted without any modifications whereas the bonded CG potentials were re-parameterized against the three pure AA melt systems (60iMA24, 60sMA15, and 50iVC24). To obtain the smoothing bonded CG potentials, all the structural distributions were smoothed by the Savitzky-Golay method.[41] As compared to the previous one that fitted these distributions to multi-Gaussian peaks,[34] this method was more in favor of exactly reproducing the target ones. In the 1:1 mapping scheme, each AA monomer of either PMMA or PVC is represented by one CG bead locating at its center of mass (COM). According to this mapping scheme, the initial AA model systems were converted to their CG counterparts, which were subjected to the CG MD simulations.

For the AA simulations, the OPLS-AA force field[42] was employed to describe the intramolecular and intermolecular interactions. Note that this force field has been used to obtain the CG potentials for PMMA.[43] The van der Waals interactions were cut-off at 1.0 nm and the dispersion corrections were employed beyond this distance whereas the Coulombic interactions were treated by the PME method.[44,45] The NVT MD (10 ns) and NPT MD (20 ns) simulations with a time step of 1 fs were performed in sequence on the AA systems. From the last 10 ns AA trajectory the target structural distributions are obtained. Within these simulation periods, the energies and densities of model systems become stable and atoms on chains have moved at least the sizes of chains (i.e., radius of gyration), which are considered as one rough criterion that systems attain equilibrium.[43,46] In particular, some preliminary calculations[35] suggest that the structural distributions used to parameterize the CG potentials seem to be insensible to the degree of equilibrium.[22] The bonded CG potentials were iteratively optimized using 20 ns CG MD simulations of small systems under the NPT ensemble, where the last 10 ns trajectories were used to

TABLE 1 Global Properties of iPMMA Chains in the Pure Systems (60iMA15) Obtained from the Experiments, AA and CG Simulations, where Data Before ± is the Averaged Value Wwhereas Data After ± is the Error Bar Representing the Standard Deviations, and the Results from AA Simulations are Based on the Center of Monomer for Comparisons

			CG	
Property	Experimental Data	AA	Previous[34,35]	Present
Density ρ (kg/m^3)	1220[50]	1051.7 ± 0.8	1281.6 ± 0.1	1123.5 ± 0.3
Radius of gyration R_g (nm)	1.08–1.10[49]	0.907 ± 0.004	0.782 ± 0.016	0.849 ± 0.019
End-to-end distance R_e (nm)	\	2.481 ± 0.024	2.010 ± 0.074	2.144 ± 0.088
Ratio $(R_e/R_g)^2$	\	7.48	6.61	6.37
Characteristic ratio $C_N = <R_e^2>/(n^*<l>^2)$[a]	10.7[49]	8.7	5.7	6.5

[a] For the CG systems, the atomistic length $<l> = 0.159$ nm and the number $n = 28$ of carbon-carbon backbone bond were used in the calculations.

abstract the structural distributions. In the parameterization step, the CG counterpart of the pure AA system was used to carry out the CG simulations.

The so-obtained CG potentials were tabulated to perform the NVT MD (10 ns) and NPT MD (100 ns) simulations on the initially mixed CG systems where the time step was 5 fs and the non-bonded CG potentials were cut-off at 1.2 nm. As confirmed in the previous work,[34] using these CG simulations polymer chains can be fully relaxed, i.e., the autocorrelation functions of end-to-end vectors decay to zero after 10 ns. Thus, the last trajectories of 90 ns CG NPT MD simulations were used to calculate various properties. For both AA and CG simulations, the Berendsen method[47] was employed to control temperature at 500 K (under NVT and NPT ensembles) and pressure at 1 atm (under NPT ensemble).

RESULTS AND DISCUSSION

CG Modeling

The accuracy of our CG potentials significantly depends upon the AA force field (i.e., OPLS-AA) used to parameterize them. This force field has been previously employed to simulate PMMA melts, reproducing the desired physical properties.[43,48] To further appreciate its validity, some conformational properties for the three pure polymer melts are computed from the AA simulations. The results are presented in Tables 1–3 together with the available experimental data. Note that our simulated results are obtained for short chains at 500 K whereas the experimental values are generally reported for high-weight chains at about 300 K.[49–51] When these factors are taken into account, our simulation results are expected to compare well with the experimental ones. More critically, tacticity effects on packing density, radius of gyration and characteristic ratio of PMMA chains have been captured by these AA simulations.

For the bonded CG potentials, only several iterations (5–6) are needed for obtaining the convergent solutions using the IBI method.[24] Since the parameterization of the nonbonded CG potentials using the CRW method are less time-consuming,[31] the whole development of the CG potentials is still computationally inexpensive. From the CG MD simulations, the intramolecular distributions up to 1–4 CG range were computed for the three pure systems, as presented in Figures 1–3 as well as the target ones obtained from the AA simulations for comparisons. It can be seen that, the resulting CG potentials exactly reproduce all the target distributions, confirming the capacity of IBI method.

However, different from the pure IBI method, the nonbonded CG potentials by our method are in advance parameterized

TABLE 2 Global Properties of sPMMA Chains in the Pure Systems (60sMA15) Obtained from the Experiments, AA and CG Simulations, where Data Before ± is the Averaged Value whereas Data After ± is the Error Bar Representing the Standard Deviations, and the Results from AA Simulations are Based on the Center of Monomer for Comparisons

			CG	
Property	Experimental Data	AA	Previous[34,35]	Present
Density ρ (kg/m^3)	1190[50]	1045.1 ± 1.7	1144.3 ± 0.1	1042.2 ± 0.2
Radius of gyration R_g (nm)	0.96–0.97[49]	0.858 ± 0.003	0.807 ± 0.016	0.873 ± 0.019
End-to-end distance R_e, (nm)	\	2.178 ± 0.018	2.082 ± 0.079	2.244 ± 0.088
Ratio $(R_e/R_g)^2$	\	6.44	6.66	6.61
Characteristic ratio $C_N = <R_e^2>/(n^*<l>^2)$[a]	9.2[49]	6.7	6.1	7.1

[a] For the CG systems, the atomistic length $<l> = 0.159$ nm and the number $n = 28$ of carbon-carbon backbone bond were used in the calculations.

TABLE 3 Global Properties of iPVC Chains in the Pure Systems (50iVC24) Obtained from the Experiments, AA and CG Simulations, where Data Before ± is the Averaged Value whereas Data After ± is the Error Bar Representing the Standard Deviations, and the Results from AA Simulations are Based on the Center of Monomer for Comparisons

			CG	
Property	Experimental Data	AA	Previous[34]	Present
Density ρ (kg/m^3)	1300–1400[50]	1245.0 ± 0.3	1544.3 ± 0.2	1389.9 ± 0.04
Radius of gyration R_g (nm)	\	1.054 ± 0.029	0.854 ± 0.011	0.933 ± 0.026
End-to-end distance R_e, (nm)	\	2.793 ± 0.173	2.129 ± 0.047	2.318 ± 0.115
Ratio $(R_e/R_g)^2$	\	7.02	6.21	6.19
Characteristic ratio $C_N=<R_e^2>/(n^*<l>^2)$[a]	7.4[51]	7.1	4.1	4.9

[a] For the CG systems, the atomistic length $<l> = 0.155$ nm and the number $n = 46$ of carbon-carbon backbone bond were used in the calculations.

using the CRW method and they are kept fixed while optimizing the bonded CG potentials.[34] As suggested by the excellent reproduction of structural distributions, the nonbonded potentials do not interfere in obtaining the convergent bonded CG potentials. Note that, the nonbonded CG potentials are independently developed to reproduce intermolecular interactions whereas the bonded CG potentials are parameterized to reproduce structural distributions, dictating their versatile ability to represent both structural and energetic properties.

Note that the radial distribution functions (RDFs) of systems are not involved in the development of CG potentials as the pure IBI method.[24] Therefore, they are natural outputs of the CG simulations that can be predicted. As shown in Figure 4, the total RDFs for all the three pure systems are presented. At distances <0.5 nm, there are two peaks for iPMMA and sPMMA, and three peaks for iPVC, which belong to the bonded peaks with the same numbers and positions as in the distributions of bond lengths [Figs. 1(a), 2(a), and 3(a)]. Except the bonded peaks, another peak at the farer distances (marked by a vertical slashed line in Fig. 4) is related to strong nonbonded interactions. The total RDFs obtained from the AA simulations are also presented in the same figures for comparisons. It can be observed that all the bonded peaks are exactly reproduced, and the nonbonded peaks exhibit some departures but the agreements are still acceptable.

As displayed in Tables 1–3, some global properties (density ρ, radius of gyration R_g, end-to-end distance R_e and characteristic ratio C_N) for the three pure systems are also computed using the CG simulations. The predicted density of pure sPMMA system using the newly developed CG potentials compares well with the target ones obtained from AA simulations, and the deviations in densities of other two pure systems are between 7 and 11%. This over-estimation seems to be one general consequence using the CRW potentials that are parameterized against single chain in vacuum,[32] which can be associated with the asphericity of monomer reduced to one CG. However, such CG potentials have the ability to reproduce the effects of chain length.[32] The values of R_g and R_e and the trend with respect to chain tacticity are not yet reproduced. Besides, all the ratios $(R_e/R_g)^2$ deviate from six as expected for Gaussian chains[22], and the characteristic ratios are somewhat lower than the results from AA simulations. Similar differences were also found in other works.[22,26] In particular, Bayramoglu and Faller have explained these differences as the different end-effects arising from the short chains.[22] Their explanations can also be suitable for our cases. Moreover, the deviation in density can shift the end-to-end distance and the radius of gyration, that is, higher density leads to lower end-to-end distance and radius of gyration.

Despite all, these properties using the newly proposed CG potentials yield better agreements with the target ones than those using the previous CG potentials.[34] Such short chains are chosen for appropriate comparisons between the AA and CG simulations. Nevertheless, as suggested by the solubility parameters,[13] such chains for PMMA are sufficient to represent a polymer. In the following section, it is demonstrated that these simple models are also adequate to capture the effects of tacticity and formulation on miscibility of the polymer blends.

Simulations of Mixed Systems

Miscibility

The intermolecular RDFs of like (PMMA/PMMA, PVC/PVC) and unlike (PMMA/PVC) pairs involved in the blend systems were computed to assess their miscibility. Some similar features to the previous work[34] can be identified. As a typical example, Figure 5 presents the results for the two equiweight or equi-mole mixed systems (i.e., 100iMA15/100iVC24 and 100sMA15/100iVC24) and the three pure systems (i.e., 60iMA15, 60sMA15, 50iVC24). It can be inferred that, upon mixing some like pairs are replaced by the unlike pairs. For each pair, whether it is like or unlike, there is one obvious peak (located at the same positions in the total RDFs for the pure systems as shown in Fig. 4), indicating strong intermolecular interactions. In addition, it can be found that the positions of these peaks are insensible to chain tacticity and they remain unchanged upon mixing.

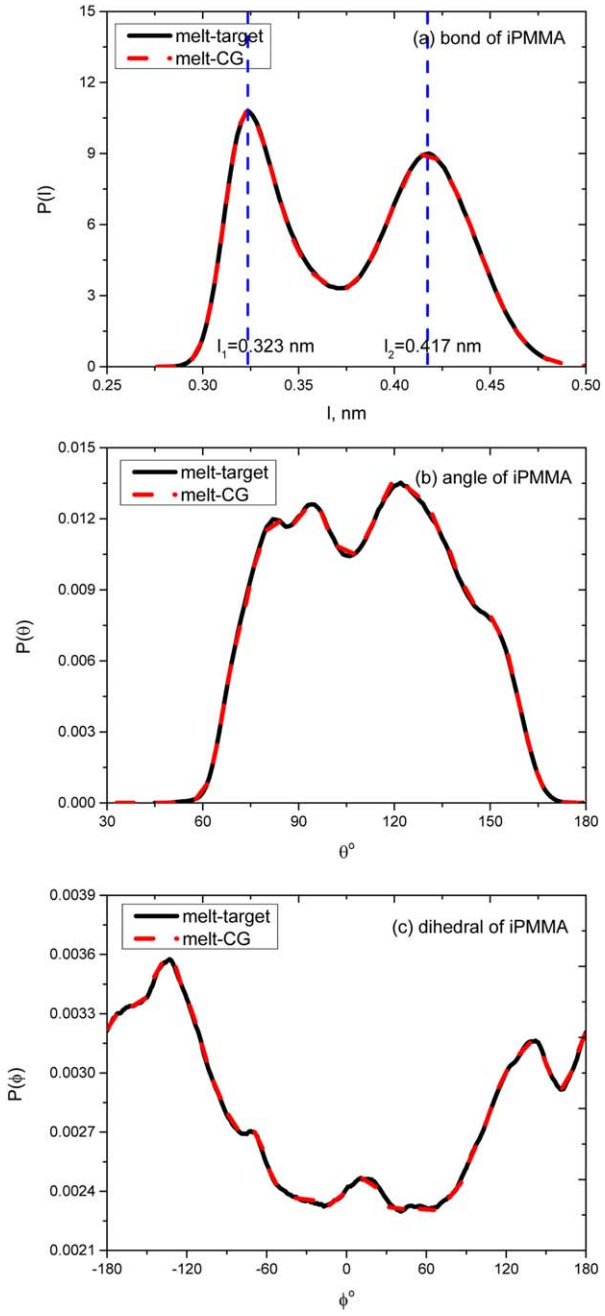

FIGURE 1 Intramolecular structural distributions of iPMMA chains in the pure system (60iMA15): CG bond (a), CG angle (b), and CG dihedral (c), where the vertical dashed lines indicate the positions of the bonded peaks. [Color figure can be viewed in the online issue, which is available at wileyonlinelibrary.com.]

Note that the peaks of the unlike pairs (PMMA/PVC) are higher than those of the like pairs (PMMA/PMMA, PVC/PVC). According to the assumption proposed by Mattice et al.[2,52] this suggests that the blend systems tend to be miscible, which agree with some experimental observations.[53–57] Besides, as compared to the cases in the iPMMA/iPVC blend, the peaks of the like pairs in the sPMMA/iPVC blend are lower and those of the unlike pairs are higher. As explained in the previous work,[34] these results strongly support the experimental observation that sPMMA is more miscible with iPVC than iPMMA.[3,58–60] Furthermore, such results are also applicable to other mixed systems with different formulations investigated in this work, indicating that the developed CG potentials are composition-transferable.

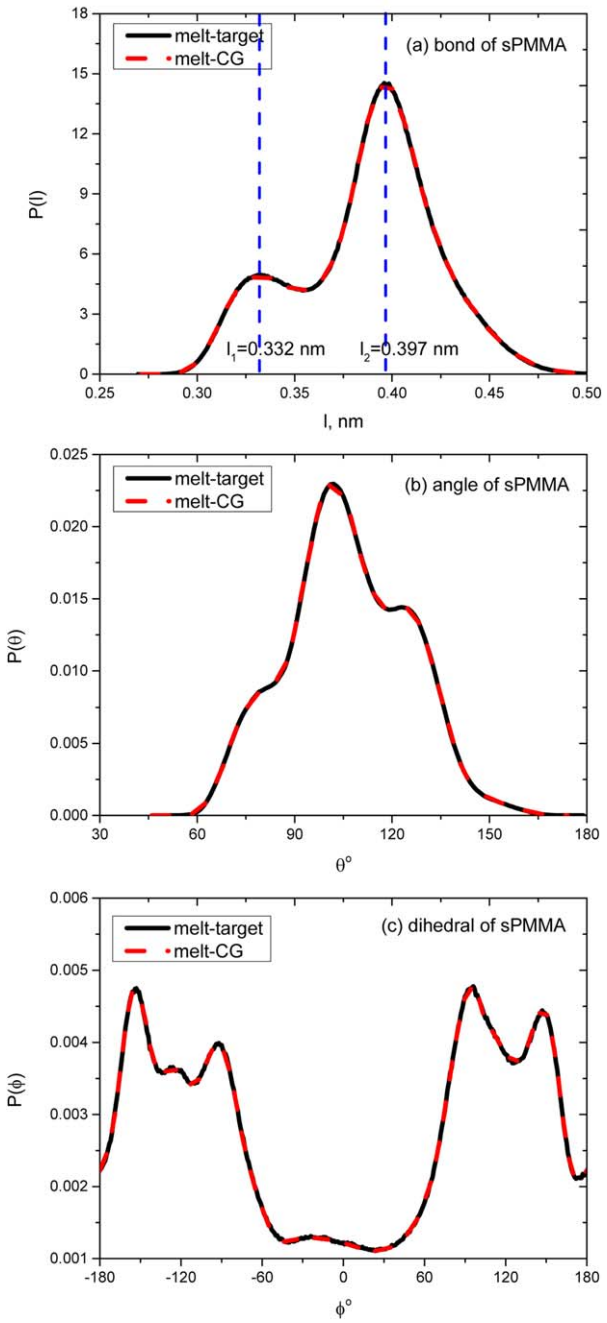

FIGURE 2 Intramolecular structural distributions of sPMMA chains in the pure system (60sMA15): CG bond (a), CG angle (b), and CG dihedral (c), where the vertical dashed lines indicate the positions of the bonded peaks. [Color figure can be viewed in the online issue, which is available at wileyonlinelibrary.com.]

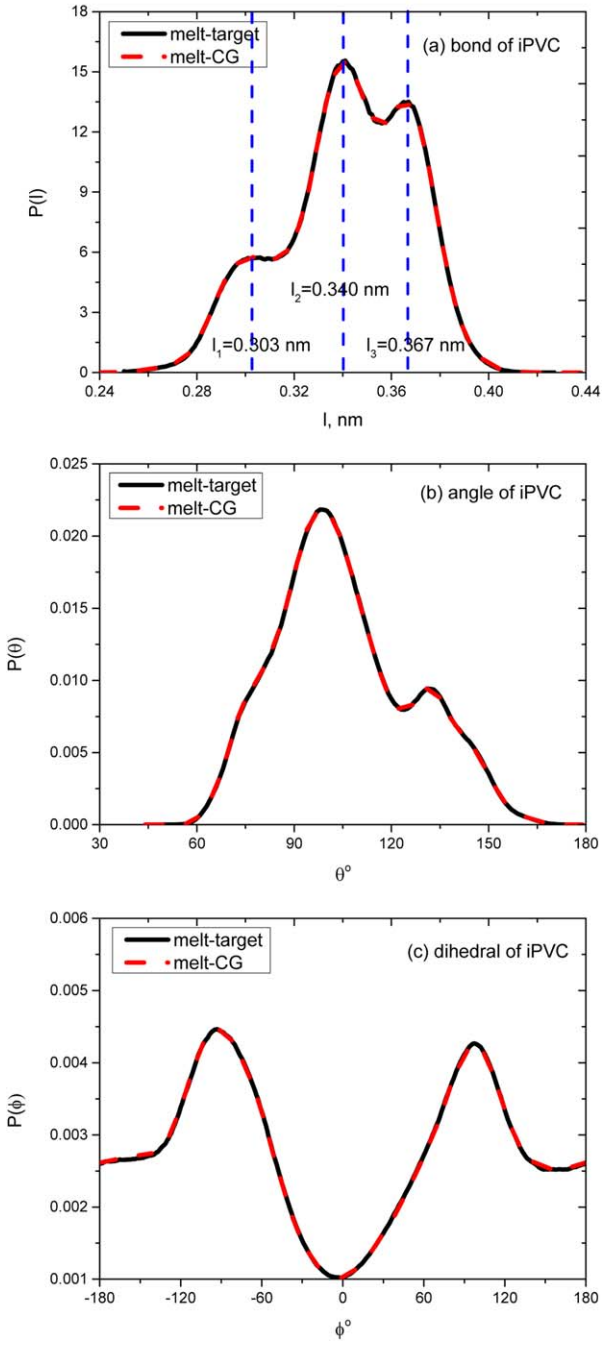

FIGURE 3 Intramolecular structural distributions of iPVC chains in the pure system (50iMA24): CG bond (a), CG angle (b), and CG dihedral (c), where the vertical dashed lines indicate the positions of the bonded peaks. [Color figure can be viewed in the online issue, which is available at wileyonlinelibrary.com.]

Mixing Effects

Although some deviations in density are found between the AA and CG simulations, the tacticity effects on the densities have been captured (Tables 1 and 2). Since the intermolecular interactions are related to density, it is instructive to disclose the tacticity effects on the changes in intermolecular interactions upon mixing and to analyze miscibility of polymer blends. Towards this, three parameters (the changes in density and volume upon mixing, and the energies of mixing) would be examined as functions of composition and chain tacticity.

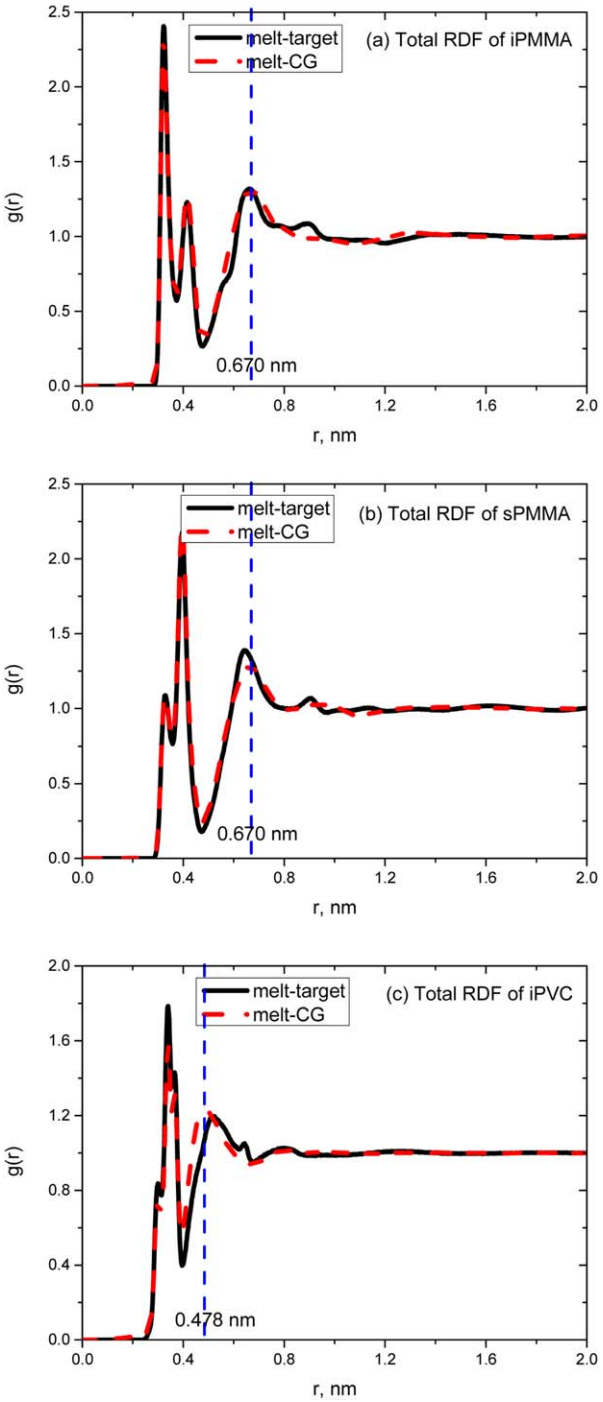

FIGURE 4 Total RDFs for the three pure systems: 60iMA15 (a), 60sMA15 (b), and 50iMA24 (c), where the vertical dashed lines indicate the positions of the nonbonded peaks. [Color figure can be viewed in the online issue, which is available at wileyonlinelibrary.com.]

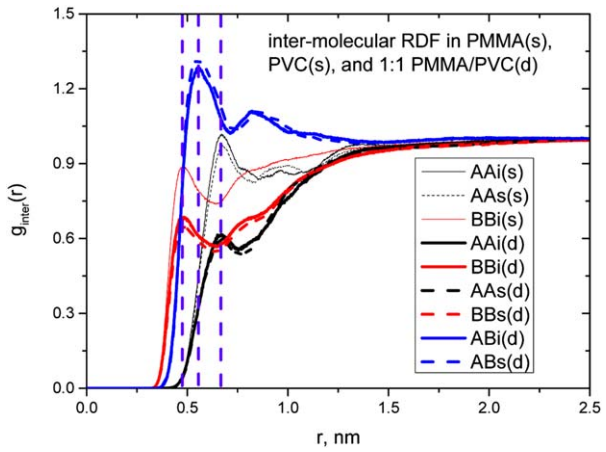

FIGURE 5 Intermolecular RDFs for three pure systems (60iMA15, 60sMA15, and 50iMA24) and two typical mixed systems (100iMA15/100iPVC and 100sMA15/100iPVC), where the pairs (AA, BB, and AB) are suffixed by one "i" or "s" to represent the cases in iPMMA/iPVC or sPMMA/iPVC and one "s" or "d" contained in a bracket denotes the cases in the single-component system (i.e., pure system) or the double-component system(i.e., mixed system), and the vertical dashed lines indicate the positions of the nonbonded peaks. [Color figure can be viewed in the online issue, which is available at wileyonlinelibrary.com.]

Changes in Density Upon Mixing. To examine the effects of compositions, the densities are computed for all the pure and mixed systems. The changes in densities upon mixing $\Delta\rho_{\mathrm{mix}}$ are then defined as

$$\Delta\rho_{mix}=\rho_{A0}\cdot\phi_A+\rho_{B0}\cdot(1-\phi_A)-\rho_{AB} \quad (1)$$

where ρ_{A0} and ρ_{B0} represent the densities of pure PMMA and PVC systems, respectively; ϕ_A is the volume fraction of component A (i.e., PMMA) in the mixed systems with densities ρ_{AB}. The volume fractions are in turn calculated from the molar volumes (V_{A0} and V_{B0}) and molar fractions (x_A) of pure components

$$\phi_A=\frac{x_A\cdot V_{A0}}{x_A\cdot V_{A0}+(1-x_A)\cdot V_{B0}} \quad (2)$$

where the molar volume is calculated from the cell volumes per chain. Note that, since chain tacticity has some effects on volumes of systems, this way can be more reasonable to calculate molecular volume than that in the previous work[34] (where the same volumes per monomer are adopted in these calculations).

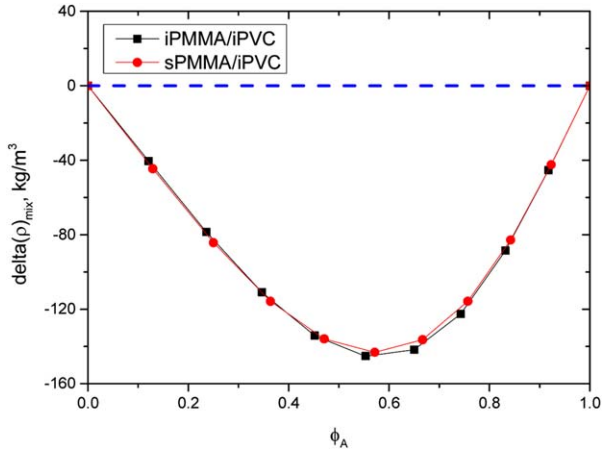

FIGURE 6 Changes in density upon mixing $\Delta\rho_{\mathrm{mix}}$ as functions of volume fractions of component A (i.e., PMMA) ϕ_A. [Color figure can be viewed in the online issue, which is available at wileyonlinelibrary.com.]

In Figure 6, the values of $\Delta\rho_{\mathrm{mix}}$ are plotted as a function of volume fraction of PMMA (that is component A) in the systems. Unless specially stated, the error bars represent the standard deviations, which are not included in the figure for clarity because they are $<1\%$ the reported values (also see Tables 1–3). It can be seen that the densities of all the mixed systems are higher than those obtained by the linear mixing rule, which is consistent with the conventional model of an interpolymer complex,[10] that is, strong interactions between distinct components lead to more densely packing. Moreover, the biggest derivation appears at around $x_A = 0.5$, indicating an optimum blend ratio.[10] However, tacticity effects cannot be obviously detected by the change in density upon mixing.

Energies of Mixing. For quantitatively evaluating miscibility, the thermodynamic interaction parameter χ is often employed. This parameter is associated with energy of mixing ΔE_{mix}, which can be calculated according to the following relation.[8,10–16,34]

$$\Delta E_{\mathrm{mix}}=E_{A0}\cdot\phi_A+E_{B0}\cdot(1-\phi_A)-E_{AB} \quad (3)$$

where E_{A0} and E_{B0} are the cohesive energy densities of pure systems *A* and *B*, respectively; E_{AB} is the cohesive energy density (CED) of mixed system, that is, the negative value of a sum of intermolecular interactions per volume; and other parameters have the same meanings as described above. Similar in style to the $\Delta\rho_{\mathrm{mix}}$, the ΔE_{mix} characterizes the changes in the CEDs of systems upon mixing. Since the smaller reference volume (i.e., monomer of PVC) is the same for all the systems, the values of ΔE_{mix} can be used for the direct comparisons.

In Figure 7, the energies of mixing for two polymer blends (iPMMA/iPVC, sPMMA/iPVC) are plotted as a function of compositions of component A. It can be observed that the energies of mixing are negative over the whole composition range, suggesting that all these systems are homogeneous. The similar curves to the plots of $\Delta\rho_{\mathrm{mix}}-\phi_A$ are obtained, which exhibit a minimum at around $x_A = 0.5$. These results are very similar to the theoretical predictions by Sato et al.[55] Moreover, at the same volume fractions more negative values in sPMMA/iPVC mean stronger interactions than in iPMMA/iPVC, which dictates the experimental observations.[3,58–60] Note that the changes in densities upon mixing result from

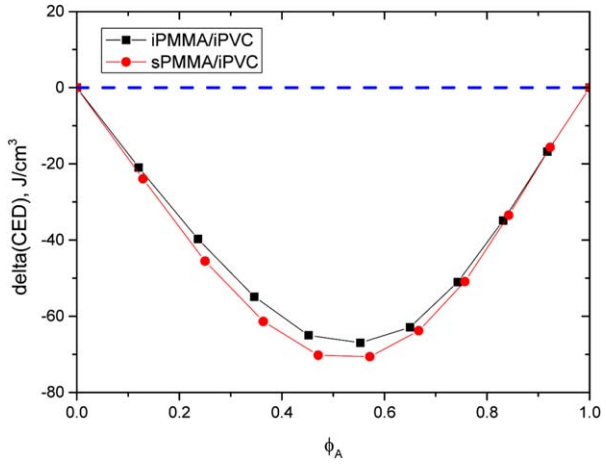

FIGURE 7 Changes in volume upon mixing ΔV_{mix} as functions of molar fractions of component A (i.e., PMMA) x_A. [Color figure can be viewed in the online issue, which is available at wileyonlinelibrary.com.]

the changes of the total volumes whereas the energies of mixing are due to the changes of both the total volumes and the intermolecular interactions. Consequently, the energies of mixing are more sensible to chain tacticity than the changes in densities upon mixing.

Changes in Volume Upon Mixing. Similarly, to detect intermolecular interactions and thus miscibility of mixing system, the change in volume upon mixing ΔV_{mix} is computed as follows

$$\Delta V_{mix} = x_A \cdot V_{A0} + (1 - x_A) \cdot V_{B0} - V_{AB} \quad (4)$$

where V_{AB} is the cell volume of mixed system, and other parameters have the same meanings as described above. The former two items mean the total volume of unit mole A and B before mixing. Note that such a piece of information can be directly achieved by the experiments, which provides a simple way to assess miscibility of polymer blends.

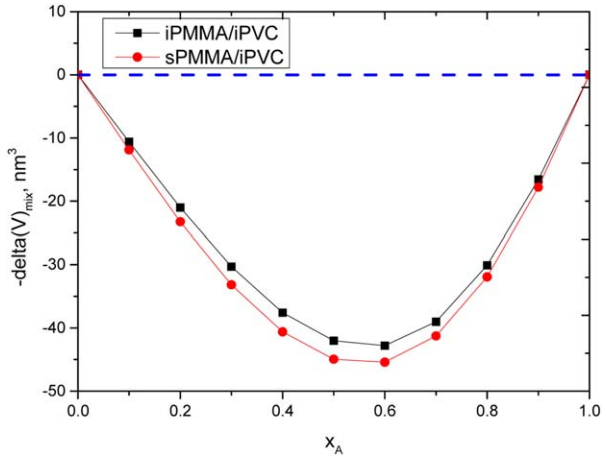

FIGURE 8 Energy of mixing ΔE_{mix} as functions of volume fractions of component A (i.e., PMMA) ϕ_A. [Color figure can be viewed in the online issue, which is available at wileyonlinelibrary.com.]

In Figure 8, the values of ΔV_{mix} are plotted as a function of molar fraction of component A in the two mixed systems. The whole curves also compare well with the theoretical predictions by Sato et al.[55] It can be seen that, upon mixing all systems undergo some shrinkages with a degree depending upon not only compositions but also chain tacticity. Moreover, there is a maximal shrinkage at $x_A = 0.5 - 0.6$, indicating an optimum blend ratio. More shrinkages mean stronger intermolecular interactions and better miscibility. Thus, these changes in volume explain the observed phase behavior. Note that total volumes include two parts, namely, the occupied volumes and the free volumes. Since the changes of the occupied volumes upon mixing are negligible, the value of ΔV_{mix} essentially suggests the changes of the free volumes. As one consequence, the free volumes are more sensible to chain tacticity than the densities.

We notice that Lemieux and coworkers have explained the miscibility of PMMA/PVC blends using the thermodynamic interaction parameter, which was in turn expressed by two contributions, that is, an interaction contribution and a free-volume contribution.[60] Furthermore, they attributed the tacticity effects on miscibility to the differences in flexibility of chains, which was related to the differences in free volumes using the Flory's equation of state theory.[59] These assumptions are quantitatively confirmed by our simulations. Regarding the characteristic ratios C_N (Tables 1–3), the simple rule "Chains of similar C_∞ tend to mix better" does not apply to our case.[3] Since the nonbonded CG potentials are almost identical for the two configurations of PMMA,[34] tacticity effects on the phase behavior of PMMA/PVC blend are mainly caused by the bonded CG potentials that determine the flexibility or accessible free volume of chains.

Mainly, this work demonstrates that the inter-molecular interaction contribution and the free-volume contribution can be quantified by ΔE_{mix} and ΔV_{mix}, respectively, which are sensible enough to reveal the effects of composition and tacticity on polymer miscibility. Note that, the theories[3,55,59] require some empirical parameters to fit to the experiments whereas our CG simulations directly obtain all values of parameters from the AA simulations (namely, no adjustable parameters are involved). Thus, this work provides some new insights into miscibility of polymer blends.

CONCLUSION

The bonded CG potentials for stereoregular PMMA/PVC blends have been reparameterized against the AA simulations of the melt systems to improve the previous CG potentials.[34] The parameterization procedure is also computationally inexpensive. With the newly developed CG potentials, the MD simulations exactly reproduce the local distributions [P(l), P(θ), P(ϕ)] of the pure systems. The simulated global properties (ρ, R_g, R_e, C_N) are also closer to the target ones than those using the previous CG potentials. It is

demonstrated that all the mixed systems are thermodynamically miscible over the whole composition range. More importantly, these simulations confirm the experimental observation that sPMMA exhibits better miscibility with iPVC than iPMMA. In addition, this work shows that the so-developed CG potentials for the PMMA/PVC blends are composition-transferable.

The curves of $\Delta\rho_{mix}$-ϕ_A, ΔV_{mix}-x_A, and ΔE_{mix}-ϕ_A, which characterize the changes in intermolecular interactions upon mixing, agree with the theoretical predictions by Sato et al.[55] A minimum at around $x_A = 0.5 - 0.6$ or $\phi_A = 0.5 - 0.6$ can be identified as well. Specially, ΔV_{mix} and ΔE_{mix} reveal the tacticity effects on miscibility but $\Delta\rho_{mix}$ does not. ΔV_{mix} is in essence related to the free volumes, and ΔE_{mix} is directly associated with the intermolecular interactions. Therefore, both of them are responsible for the observed phase behaviors. At last but not least, the developed CG potentials, which well describe both intra-molecular structure and intermolecular interactions, significantly contribute to these new insights into miscibility of polymer blends. It is expected that such models and methods would be widely used to quickly optimize the formulations of polymer blends.

ACKNOWLEDGMENTS

This work is supported by the National Natural Science Foundation of China (NSFC) under grant 21104018/B040613, and the Innovative Research Team in Higher Educational Institute of Hunan Province, and the Training Plan for Young Backbone Teachers of Hunan Province, and the Talent Support Plan of Hunan University of Humanities Science & Technology (HUHST). The author is indebted to the Molecular Simulation Center of Hunan Province (situated at Hunan University), which provides the commercial software (Materials Studio-4.0) to build the initial structural models, and the Laboratory for High Performance Computing (HPC) of the Key Discipline "Computer Applied Techniques" of Hunan Province (located at HUHST), which provides the generous CPU times for completing this work.

REFERENCES AND NOTES

1 J. F. Parmer, L. C. Dickinson, J. C. W. Chien, R. S. Porter, *Macromolecules* **1989**, *22*, 1078–1083.

2 W. L. Mattice, C. A. Helfer, S. S. Rane, E. D. von Meerwall, B. L. Farmer, *J. Polym. Sci. Part B: Polym. Phys.* **2005**, *43*, 1271–1282.

3 J. D. Honeycutt, *Macromolecules* **1994**, *27*, 5377–5381.

4 F. H. Case, J. D. Honeycutt, *Trends Polym. Sci.* **1994**, *2*, 259–266.

5 C. F. Fan, B. D. Olafson, M. Blanco, S. L. Hsu, *Macromolecules* **1992**, *25*, 3667–3676.

6 C. Qian, S. Grigoras, L. D. Kennan, *Macromolecules* **1996**, *29*, 1260–1265.

7 K. Choi, W. H. Jo, *Macromolecules* **1997**, *30*, 1509–1514.

8 S. S. Patnailk, R. Pachter, *Polymer* **2002**, *43*, 415–424.

9 P. Gestoso, J. Brisson, *Polymer* **2003**, *44*, 2312–2329.

10 F. S. Moolman, M. Meunier, P. W. Labuschagnea, P.-A. Truter, *Polymer* **2005**, *46*, 6192–6200.

11 H. Ren, Q. Zhang, X. Chen, W. Zhao, J. Zhang, H. Zhang, R. Zeng, S. Xu, *Polymer* **2007**, *48*, 887–893.

12 T. Spyriouni, C. Vergelati, *Macromolecules* **2001**, *34*, 5306–5316.

13 S. S. Jawalkar, S. G. Adoor, Malladi Sairam, M. N. Nadagouda, T. M. Aminabhavi, *J. Phys. Chem. B* **2005**, *109*, 15611–15620.

14 S. S. Jawalkar, K. V. S. N. Raju, S. B. Halligudi, M. Sairam, T. M. Aminabhavi, *J. Phys. Chem. B* **2007**, *111*, 2431–2439.

15 C. Gu, H. Gu, M. Lang, *Macromol. Theory Simul.* **2013**, *22*, 377–384.

16 Z. Luo, J. Jiang, *Polymer* **2010**, *51*, 291–299.

17 Y. Fu, L. Liao, L. Yang, Y. Lan, L. Mei, Y. Liu, S. Hu, *Mol. Simul.* **2013**, *39*, 415–422.

18 G. A. Voth, Coarse-Graining of Condensed Phase and Biomolecular Systems; CRC Press: New York, **2009**.

19 F. Muller-Plathe, *ChemPhysChem* **2002**, *3*, 754–769.

20 H. A. Karimi-Varzaneh, F. Muller-Plathe, *Top. Curr. Chem.* **2012**, *307*, 295–322.

21 E. Brini, E. A. Algaer, P. Ganguly, C. Li, F. Rodrıguez-Ropero, N. F. A. van der Vegt, *Soft Matter* **2013**, *9*, 2108–2119.

22 B. Bayramoglu, R. Faller, *Macromolecules* **2012**, *45*, 9205–9219.

23 B. Bayramoglu, R. Faller, *Macromolecules* **2013**, *46*, 7957–7976.

24 D. Reith, M. Putz, F. Muller-Plathe, *J. Comput. Chem.* **2003**, *24*, 1624–1636.

25 Q. Sun, R. Faller, *J. Chem. Theory Comput.* **2006**, *2*, 607–615.

26 P. Carbone, H. A. K. Varzaneh, X. Chen, F. Müller-Plathe, *J. Chem. Phys.* **2008**, *128*, 064904.

27 C.-C. Fu, P. M. Kulkarni, M. S. Shell, L. G. Leal, *J. Chem. Phys.* **2012**, *137*, 164106.

28 Q. Sun, R. Faller, *J. Chem. Phys.* **2007**, *126*, 144908.

29 C.-K. Lee, C.-W. Pao, C.-W. Chu, *Energy Environ. Sci.* **2011**, *4*, 4124–4132.

30 J.-M. Y. Carrillo, R. Kumar, M. Goswami, B. G. Sumpter, W. M. Brown, *Phys. Chem. Chem. Phys.* **2013**, *15*, 17873–17882.

31 E. Brini, V. Marcon, N. F. A. van der Vegt, *Phys. Chem. Chem. Phys.* **2011**, *13*, 10468–10474.

32 E. Brini, N. F. A. van der Vegt, *J. Chem. Phys.* **2012**, *137*, 154113.

33 H. A. Karimi-Varzaneh, N. F. A. van der Vegt, F. Muller-Plathe, P. Carbone, *ChemPhysChem* **2012**, *13*, 3428–3439.

34 C. Wu, *Macromolecules* **2013**, *46*, 5751–5761.

35 C. Wu, *J. Mol. Mod.* **2014**, *20*, 2377.

36 J. M. Martinez, L. Martinez, *J. Comput. Chem.* **2003**, *24*, 819–825.

37 L. Martinez, R. Andrade, E. G. Birgin, J. M. Martinez, *J. Comput. Chem.* **2009**, *30*, 2157–2164.

38 V. Ruhle, C. Junghans, A. Lukyanov, K. Kremer, D. Andrienko, *J. Chem. Theory Comput.* **2009**, *5*, 3211–3223.

39 D. van der Spoel, E. Lindahl, B. Hess, G. Groenhof, A. E. Mark, H. J. C. Berendsen, *J. Comput. Chem.* **2005**, *26*, 1701–1718.

40 B. Hess, C. Kutzner, D. van der Spoel, E. Lindahl, *J. Chem. Theory Comput.* **2008**, *4*, 435–447.

41 P. A. Gorry, *Anal. Chem.* **1990**, *62*, 570–573.

42 W. L. Jorgensen, D. S. Maxwell, J. Tirado-Rives, *J. Am. Chem. Soc.* **1996**, *118*, 11225–11236.

43 C. Chen, P. Depa, J. K. Maranas, V. G. Sakai, *J. Chem. Phys.* **2008**, *128*, 124906.

44 T. Darden, D. York, L. Pedersen, *J. Chem. Phys.* **1993**, *98*, 10089–10092.

45 U. Essmann, L. Perera, M. L. Berkowitz, T. Darden, H. Lee, L. G. Pedersen, *J. Chem. Phys.* **1995**, *103*, 8577–8592.

46 K. Karatasos, *Macromolecules* **2005**, *38*, 4472–4483.

47 H. J. C. Berendsen, J. P. M. Postma, W. F. van Gunsteren, A. DiNola, J. R. Haak, *J. Chem. Phys.* **1984**, *81*, 3684–3690.

48 N. Metatla, A. Soldera, *Mol. Simul.* **2006**, *32*, 1187–1193.

49 J. M. O'Reilly, D. M. Teegarden, G. D. Wignall, *Macromolecules* **1985**, *18*, 2747–2752.

50 B. Ellis, R. Smith, Polymers-a property datbase, 2nd ed.; CRC Press: New York, **2009**.

51 J. Bicerano, Prediction of Polymer Properties; Marcel Deeker, Inc.: New York, **2002**.

52 T. C. Clancy, M. P. tz, J. D. Weinhold, J. G. Curro, W. L. Mattice, *Macromolecules* **2000**, *33*, 9452–9463.

53 M. S. Khan, R. A. Qazi, M. S. Wahid, *Afr. J. Pure Appl. Chem* **2008**, *2*, 041–045.

54 D. J. Walsh, G. L. Cheng, *Polymer* **1984**, *25*, 499–502.

55 T. Sato, Y. Tsujita, A. Takizawa, T. Kinoshita, *Macromolecules* **1991**, *24*, 158–160.

56 K. Karlou, H. A. Schneider, *J. Therm. Anal. Cal.* **2000**, *59*, 59–69.

57 C. Lau, Y. Mi, *J. Polym. Sci. Part B: Polym. Phys.* **2001**, *39*, 2390–2396.

58 J. W. Schurer, A. d. Boer, G. Challa, *Polymer* **1975**, *16*, 201–204.

59 E. J. Vorenkamp, G. t. Brinke, J. G. Meijer, H. Jager, G. Challa, *Polymer* **1985**, *26*, 1725–1732.

60 E. Lemieux, R. E. Prud'homme, R. Forte, R. Jerome, P. Teyssie, *Macromolecules* **1988**, *21*, 2148–2154.